ELSEVIER

Contents lists available at ScienceDirect

## Inorganica Chimica Acta

journal homepage: www.elsevier.com/locate/ica





# Synthesis, structural characterization, and corrosion inhibition properties of rare earth 2-hydroxyphenylacetate coordination polymers<sup>☆</sup>

Naveena Y. Salpadoru Thuppahige <sup>a</sup>, Zhifang Guo <sup>a</sup>, Glen B. Deacon <sup>b</sup>, Peter C. Junk <sup>a,\*</sup>

- <sup>a</sup> College of Science & Engineering, James Cook University, Townsville, QLD 4811, Australia
- <sup>b</sup> School of Chemistry, Monash University, Clayton, VIC 3800, Australia

#### ARTICLE INFO

Keywords:
Rare earth metals
Carboxylates
2-Hydroxyphenylacetate
Crystal structures
Corrosion inhibitors
Mild steel

#### ABSTRACT

The salt metathesis reaction between sodium 2-hydroxyphenylacetate (Na(2hpa)) and a rare earth (RE) metal nitrate or chloride in an aqueous ethanol medium has yielded a series of rare earth one-dimensional (1-D) coordination polymers  $[La(2hpa)_3(H_2O)_2]_n$  (1),  $\{[RE_2(2hpa)_6(H_2O)_4]\cdot 3.5H_2O\}_n$  (RE = Ce (2), Nd (3)), and  $\{[RE_2(2hpa)_6(H_2O)_2]\cdot 3H_2O\}_n$  (RE = Gd (4), Dy (5), Y (6), Er (7), Yb (8)) which have three different crystal structures. All structures were determined by single-crystal X-ray diffraction (XRD), except Y (6) and Yb (8) compounds, which were isomorphous with Gd (4), Dy (5), and Er (7) complexes by their unit cell parameters and X-ray powder diffraction (XRPD) patterns. Only the La complex (1) has a mononuclear repeating unit while the others are based on binuclear units. The chelating bridging carboxylate coordination mode is common for all complexes. In addition, complexes 1-3 exhibit the chelating mode with the 10-coordination number whereas complexes 4-8 have syn-syn-bridging bidentate binding with the coordination number of 9. In the weight loss anti-corrosion experiments, the  $\{[Gd_2(2hpa)_6(H_2O)_2]\cdot 3H_2O\}_n$  (4) compound demonstrated the highest inhibition efficiency of 57 %. A significant difference between RE 2-hydroxyphenylacetate complexes and [Ce(sal-H)<sub>3</sub>(H<sub>2</sub>O)]<sub>n</sub> was usually not observed indicating little impact of the -CH<sub>2</sub>- unit between carboxylate and benzene ring. The reduced corrosion inhibition efficiencies of RE 2-hydroxyphenylacetate complexes compared with RE 4-hydroxyphenylacetates confirm the positive effect of the p-OH group on the benzene ring on anti-corrosion properties.

## 1. Introduction

Rare earth metal complexes are mainly formed by trivalent ions as it is the most stable oxidation state, and their hard acid nature particularly favours oxygen donors [1,2]. Carboxylates typically exhibit a wide range of binding modes resulting in many and various structural arrangements with rare earth metals [3,4]. These complexes have the potential to be used in different applications such as catalysis [5], luminescence [6], bioimaging [7], NMR shift reagents [8], proton-conducting materials [9] and also as corrosion inhibitors [10,11]. Among rare earth carboxylates, 2-hydroxybenzoates (salicylates) have a special place from a structural viewpoint [12]. Not only do the hydrates form four structural classes (two polymeric types, dimers, and monomers), but most metals crystallize in at least two forms from water, whilst holmium gives crystals of a monomer, a dimer and a polymer. For

the larger metals, coordination of the OH group is observed in the polymeric structure, but not in the other three structural types [12]. By contrast, rare earth phenylacetate hydrates have only two structural types, with the larger metals (La—Ho) forming a nine coordinate polymer and Y—Lu a polymer with three eight coordinate metal atoms and one nine [13]. In this paper, we examine whether the introduction of a 2-hydroxy substituent into the phenylacetate ligand introduces more structural variety.

Rare earth carboxylate complexes are considered as promising candidates as corrosion inhibitors, since the innovation of cerium salicylate in 2002 [10,14–16]. The cerium complex is a double-stranded polymeric structure, [Ce(salH) $_3$ (H $_2$ O)] $_n$  with three different modes of coordination of the salicylate ligands [12]. Due to the dual anodic and cathodic inhibition action of this complex against corrosion, research on the anticorrosion properties of rare earth carboxylate compounds has been

E-mail address: peter.junk@jcu.edu.au (P.C. Junk).

<sup>\*</sup> This article is part of a Special issue entitled: 'Glen Deacon' published in Inorganica Chimica Acta. We dedicate this paper to Professor Glen Deacon for his stellar contributions to a wide variety of chemistry spanning more than seven decades. He has been a phenomenal influence to the discipline and many of his co-workers and students..

 $<sup>^{\</sup>star}$  Corresponding author.

growing for the past two decades [10,16]. The excellent performance of those novel RE complexes in protecting some steel and aluminium alloys against corrosion has proven as an effective alternative for the toxic chromate compounds, which are the best known commercially used inhibitors [16,17] but are being phased out.

After cerium salicylate, rare-earth carboxylates with different structural motifs have been synthesized to study their anticorrosion properties and lanthanum 4-hydroxycinnamate [18], yttrium 3-(4'-methylbenzoyl)propionate [19,20], yttrium 3-furoate [21], yttrium and lanthanum 4-hydroxybenzoate [22], and 3-thiophenecarboxylate [23] were identified as excellent inhibition compounds. However, some RE carboxylate complexes such as complexes of 3-(4'-hydroxyphenyl)-propionate [24], phenylacetate [13], and 2-methyl-3-furoate [17] did not achieve high inhibition levels. A recent study on the anticorrosion properties of rare earth 4-hydroxyphenylacetate complexes, indicated the advantage of adding the *p*-OH group to the structure [25]. Thus, the effect of the presence of an *o*-OH group on the benzene ring in terms of corrosion inhibition properties is interesting to determine the impact of the location of the -OH functionality on the structure.

Moreover, 2-hydroxyphenylacetate (Fig. 1(a)) has a -CH $_2$ - group between the benzene ring and the -COO $^-$  group of the salicylate ion (Fig. 1(b)). Comparison of the structural changes and corrosion inhibition capabilities of the RE 2-hydroxyphenylacetate complexes with those of cerium salicylate, which has significantly influenced research on RE carboxylates corrosion inhibition, is important for studying structure-activity relationship in this inhibitor class.

#### 2. Results and discussion

## 2.1. Synthesis and characterization

The salt metathesis reaction between sodium 2-hydroxyphenylacetate (2hpa) and the selected rare-earth nitrate or chloride in an aqueous medium with a little ethanol yielded the rare earth 2-hydroxyphenylacetate aqua complexes as shown in Scheme 1.

During the salt metathesis reaction, a precipitate (bulk sample) was obtained only for the compounds of La, and Ce. For other compounds, slightly cloudy solutions were obtained and there was not enough powder to collect. Crystalline samples were collected from the mother liquor by slow evaporation. Crystal structures were determined for La (1), Ce (2), Nd (3), Gd (4), Dy (5), and Er (7) complexes from single crystal data. Owing to the poor quality of the crystals of the Y (6) and Yb (8) complexes, the structures could not be determined. However, their unit cell parameters (see experimental section) and powder patterns showed they were isomorphous with the compounds 4, 5, and 7. The powder patterns of the other compounds were comparable with their

simulated powder patterns derived from the Mercury software based on the single crystal X-ray data (Fig. S4), thereby confirming bulk identity.

In TGA graphs of all **1–8** compounds, the first weight loss step corresponds with the loss of both coordinated and lattice water (Fig. S5). The temperature range of this step starts from room temperature (around 25 °C) to 105–115 °C and for compound **4**, it was up to 150 °C. The second weight loss around 110–300 °C was obtained as  $\sim\!25–27$  % for all compounds except the complexes **1** and **6**, which exhibited a weight loss of  $\sim\!31–34$  % from 110 to 265 °C. The second weight loss stage for all compounds **1–8** was consistent with the removal of an (o-HO-C<sub>6</sub>H<sub>4</sub>-CH<sub>2</sub>)<sub>2</sub>CO (R<sub>2</sub>CO) ketone and formation of a carboxylatocarbonate complex (Eq. 1). The data are given in Table S8, where some variation between calculated and found values may be attributed to some uncertainty in selection of the end temperature of the second weight loss (Fig. S5).

$$4RE(O_2CR)_3 \rightarrow RE_4(O_2CR)_6(CO_3)_3 + 3R_2CO$$
 (1)

The IR spectra of all 1-8 compounds showed similar patterns while isostructural compounds exhibit almost identical spectra having similar peaks at the same wavelengths or with slight deviation (Table 1; Fig. S7). Several main peaks corresponding to the functional groups of the complexes, can be identified. The O—H stretching vibrations of coordinated and lattice water molecules, as well as the hydroxyl group of the ligand contribute to the broad bands at 3050–3550 cm<sup>-1</sup> in the spectra [26]. A prominent strong peak (at 1687 cm<sup>-1</sup> in the free acid spectrum; Fig. S6) corresponding to the absorption band of the carbonyl group was absent in all compounds, indicating the coordination of -COO- through deprotonation of -COOH [27]. Asymmetric and symmetric stretching vibration bands related to the carboxylate group of all compounds are observed at 1589–1517 cm<sup>-1</sup> and 1406–1425 cm<sup>-1</sup> respectively. Moreover, having a lower value for the difference between asymmetric and symmetric vibrations ( $\Delta \nu$ ), than its ionic value, suggests that the presence of the bridging and/or chelating carboxylate groups and the absence of the unidentate coordination mode for the complexes [28,29] (Table 1).

## 2.2. Crystal and molecular structures

Three different structural classes were obtained, namely [La  $(2hpa)_3(H_2O)_2]_n$  (1),  $\{[RE_2(2hpa)_6(H_2O)_4]\cdot 3.5H_2O\}_n$  (RE = Ce (2), Nd (3)), and  $\{[RE_2(2hpa)_6(H_2O)_2]\cdot 3H_2O\}_n$  (RE = Gd (4), Dy (5), Y (6), Er (7), Yb (8)), in contrast to two for unsubstituted phenylacetate [13]. The crystallographic and refinement data are given in the supporting information in Table S1. Only three types of carboxylate coordination modes are observed in all of 1–8 as shown in Fig. 2. No coordination of the hydroxyl group was observed unlike ligation of salicylate [12]. Although

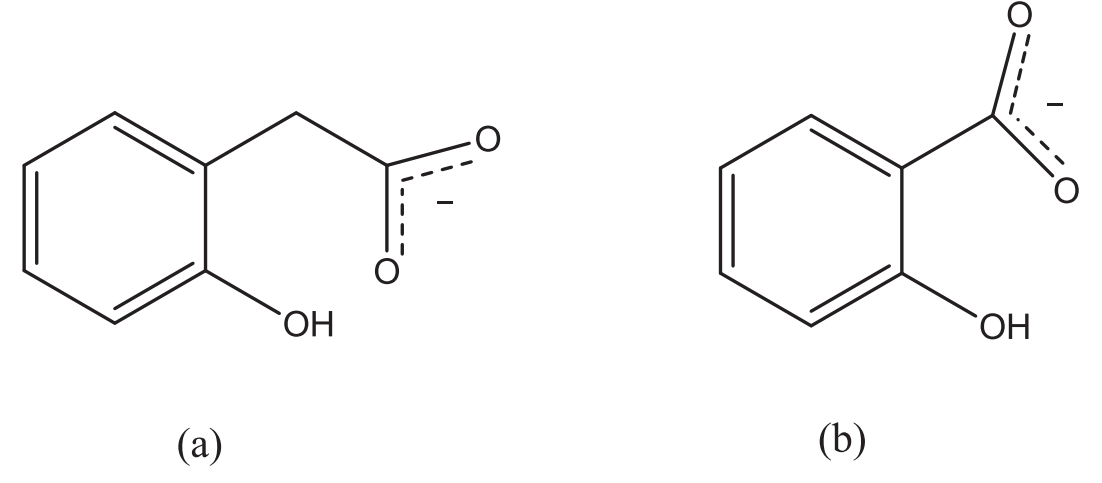


Fig. 1. Structures of (a) 2-hydroxyphenylacetate and (b) salicylate ion.

3 Na(2hpa) + RE(X)<sub>3</sub>·xH<sub>2</sub>O 
$$\xrightarrow{\text{H}_2\text{O/EtOH}}$$
 {[RE(2hpa)<sub>3</sub>(H<sub>2</sub>O)<sub>y</sub>]·zH<sub>2</sub>O}<sub>n</sub> + 3 NaX  
2hpa = 2-Hydroxyphenylacetate  $y = 2, z = 0; RE = \text{La (1)}$   
 $X = \text{NO}_3$ -, Cl<sup>-</sup>  $y = 4, z = 3.5; RE = \text{Ce (2)}, \text{Nd (3)}$   
 $x = \text{Water molecules coordinated and}$   
lattice respectively

Scheme 1. Synthesis of RE 2-hydroxyphenylacetate complexes by salt metathesis reactions.

 $\begin{tabular}{ll} \textbf{Table 1} \\ \textbf{Selected infrared bands (cm}^{-1}) \ of the RE 2-hydroxyphenylacetate complexes. \\ \end{tabular}$ 

Compound	ν(OH) water	$\nu_{\rm as}({\rm CO}_2^-)$	$\nu_{\rm s}({\rm CO}_2^-)$	$\Delta \nu = ( u_{as} -  u_{s})avg$	$\delta(\mathrm{CO}_2^-)$
Na(2hpa)	3070	1592,	1413,	161	_
		1562,	1374		
		1508			
$[La(2hpa)_3(H_2O)_2]_n$ (1)	3226	1584,	1406	143	647
		1546,			
		1517			
$\{[Ce_2(2hpa)_6(H_2O)_4]\cdot$	3277	1586,	1417	135	651
$3.5H_2O_n$ (2)		1551,			
		1519			
$\{[Nd_2(2hpa)_6(H_2O)_4]\cdot$	3269	1586,	1425	127	659
$3.5H_2O_n$ (3)		1551,			
		1519			
$\{[Gd_2(2hpa)_6(H_2O)_2]\cdot$	3153	1589,	1419	140	626
$3H_2O_n$ (4)		1561,			
		1527			
$\{[\mathrm{Dy_2}(\mathrm{2hpa})_6(\mathrm{H_2O})_2]\cdot$	3159	1589,	1421	140	626
$3H_2O_n$ (5)		1566,			
		1527			
$\{[Y_2(2hpa)_6(H_2O)_2]\cdot$	3171	1589,	1425	137	626
3H <sub>2</sub> O} <sub>n</sub> ( <b>6</b> )		1570,			
		1528			
$\{[Er_2(2hpa)_6(H_2O)_2]\cdot$	3157	1589,	1421	140	626
3H <sub>2</sub> O} <sub>n</sub> (7)		1567,			
		1527			
{[Yb <sub>2</sub> (2hpa) <sub>6</sub> (H <sub>2</sub> O) <sub>2</sub> ]·	3153	1570,	1425	124	626
$3H_2O_n$ (8)		1528			

this might be attributed to the need of a 7-membered chelate ring for 2hpa, the RE ions are large enough to accommodate this.

[La(2hpa)<sub>3</sub>(H<sub>2</sub>O)<sub>2</sub>]  $_{n}$ : The lanthanum complex forms a mononuclear derived 1-D polymeric chain, and it crystallizes in the monoclinic crystal system and  $P2_1/n$  space group. The asymmetric unit of the complex consists of three ligands and two coordinated water molecules, and the asymmetric unit and a part of its polymeric chain are depicted in Fig. 3.

The La<sup>III</sup> metal ion is 10 coordinate with five ligands and two water molecules resulting in a bicapped square antiprismatic geometry. Among the five ligands, the chelating  $\kappa(O,O')$  (ii) ligand is connected through two oxygens (O1, O2) and the other four ligands show the *synsyn* chelating bridging  $Z,Z-\mu-1\kappa(O):2\kappa(O,O')$  (iii) mode through  $(O4^*,5^*)$ ,  $(O7^*,8^*)$ , O4, and O7. The two water molecules (O10,11) are *cisoid* coordinated with an O10-La1-O11 angle of  $68.06(11)^\circ$ . Two metal ions are bridged through two chelating bridging ligands to make a polymeric chain with the separations of 4.3159(6) Å  $(La1^*-La1)$  and 4.3661(6) Å  $(La1^*-La1)$  between adjacent metal ions and a La1\*-La1-La1\* angle of  $172.978(14)^\circ$ . The bridging oxygens O7 and O7\* form a  $113.32(11)^\circ$  angle  $(La1-O7-La^*$  and  $La1-O7^*-La^*$ ), while the bridging angle at O4 and O4\*  $(La1-O4-La^*$  and  $La1-O4^*-La^*$ ) is  $114.86(12)^\circ$  (Table S2).

The La—O bond lengths of the complex are listed in the caption of Fig. 3 and in Table S2. The average La—O bond length of carboxylates along the chain is 2.594 Å and it is shorter than that of coordinated  $\rm H_2O$  (2.612 Å). Moreover, five different intramolecular H bonds can be observed within the chain. Two of them are formed by a coordinated water oxygen atom O11, with a carboxylate (O2\*) and a hydroxyl (O3#) from ligands bound to adjacent metal centers. The other three H-bonds arise from three different hydroxyl oxygens acting as donor atoms to coordinated carboxylate oxygens. Only O3-H3...O1 exhibits an intramolecular hydrogen bond within the asymmetric unit, while O6 and O9

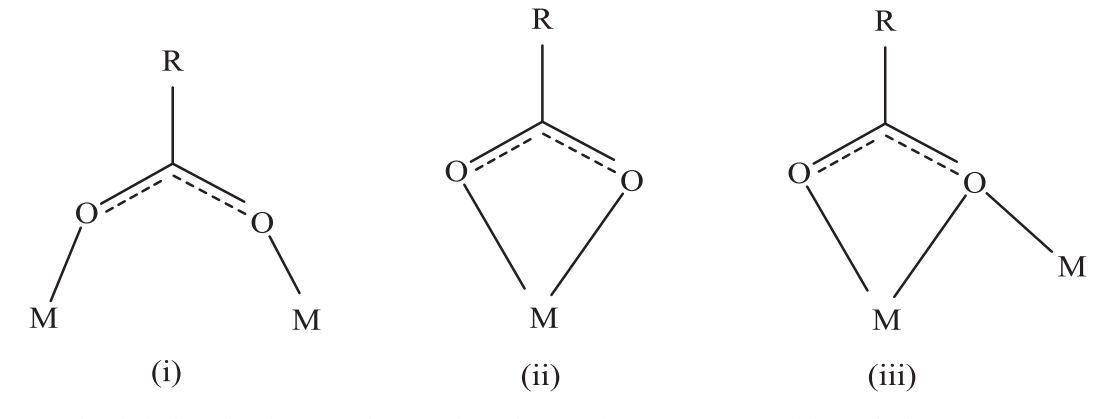


**Fig. 2.** Coordination modes of 2-hydroxyphenylacetate with rare earth metals in complexes 1–8: (i) syn,syn- bidentate bridging - Z,Z-μ-1κ(O):2κ(O'); (ii) chelating - κ(O,O'); (iii) chelating bridging - Z,Z-μ-1κ(O):2κ(O,O').

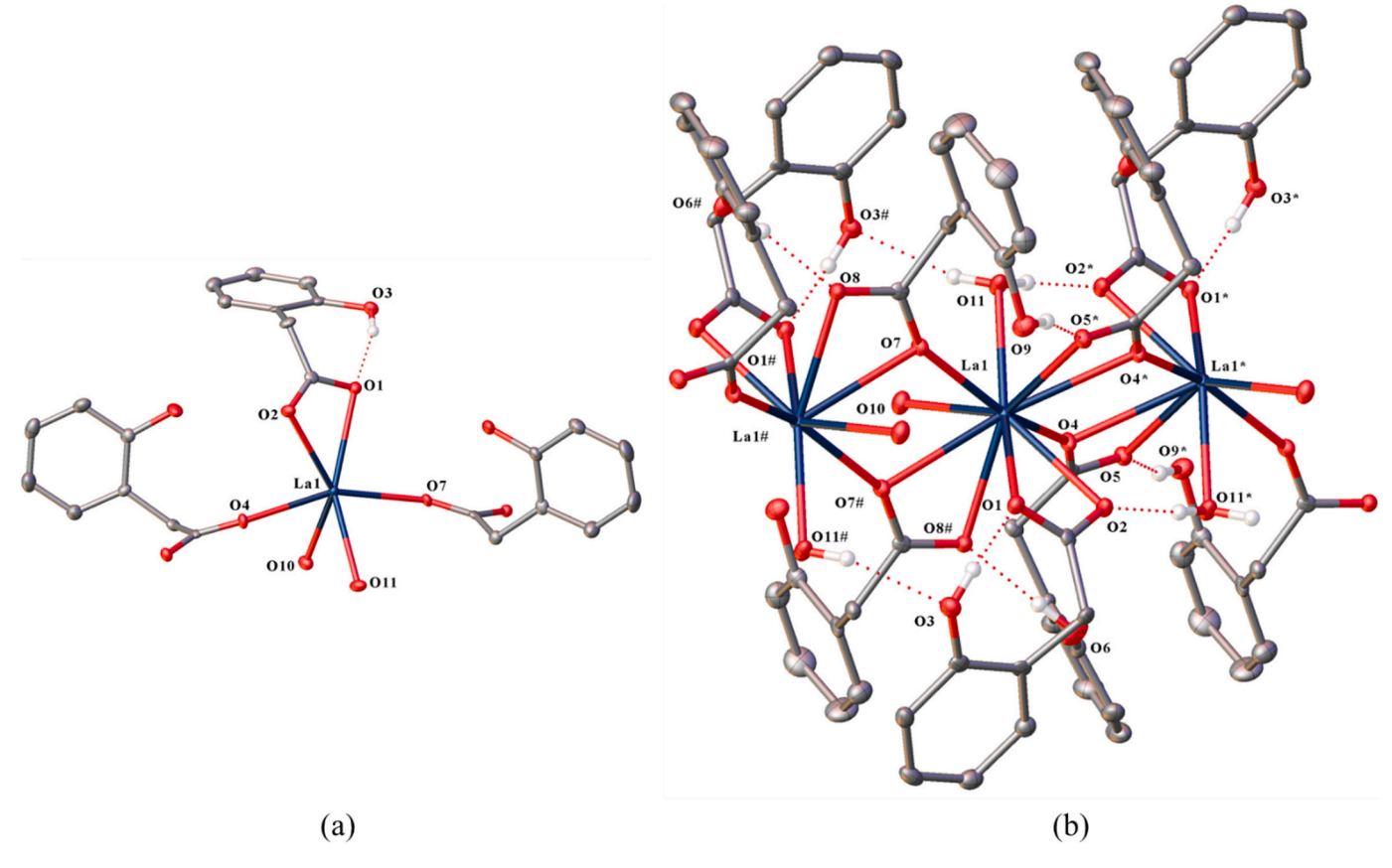


Fig. 3. (a) The asymmetric unit of complex 1; (b) Part of the polymeric chain with 50 % thermal ellipsoids. Dotted lines indicate the intra-molecular hydrogen bonds. The hydrogen atoms, except those contributing to hydrogen bonds, are omitted for clarity. Selected bond lengths (Å); 1: La1-O1 2.6728(3), La1-O2 2.56980(17), La1-O4 2.48951(14), La1-O72.49414(16), La1-O10 2.67094(18), La1-O11 2.55265(19), La1-O4\* 2.68991(18), La1-O5\* 2.5998(2), La1-O7# 2.67075(17), La1-O8# 2.5654(2). Symmetry codes: \*1-X, 1-Y, 1-Z; #2-X, 1-Y, 1-Z.

hydroxyl oxygens form H-bonds with carboxylate O8# and O5\* respectively, of adjacent ligands. All H bond lengths and angles of [La  $(2hpa)_3(H_2O)_2]_n$  are listed in Table S3. In contrast with the other two structural types, interchain interactions are not present in this structure (Fig. S1).

 $\{[RE_2(2hpa)_6(H_2O)_4]\cdot 3.5H_2O\}_n \ (RE=Ce\ (2),\ Nd\ (3)):$  Complexes 2 and 3 are isomorphous with two unique metal ions along the one-dimensional polymeric structure. Both complexes crystallize in a triclinic crystal system with a P-1 space group. The asymmetric unit comprises two metal centers with different coordination spheres, six carboxylate ligands, four ligated water molecules, and 3.5 waters of crystallization associated with H bonds in the crystal lattice. The asymmetric unit and a segment of the structure of 3 showing the two different coordination environments are shown in Fig. 4.

Only the chelating  $\kappa(O,O')$  (iii) and syn-syn chelating bridging Z,Z- $\mu\text{-}1\kappa(O):2\kappa(O,O')$  (iii) carboxylate modes are observed in these complexes. Both Nd1 and Nd2 metal centers are surrounded by one  $\kappa(O,O')$  (ii) and four Z,Z- $\mu\text{-}1\kappa(O):2\kappa(O,O')$  (iii) carboxylates and two cisoid water ligands resulting in a ten-coordinated bicapped square antiprismatic geometry. The Nd1 ion is bound by the  $\kappa(O,O')$  (ii) carboxylate ligand through (O1,2) and by the Z,Z- $\mu\text{-}1\kappa(O):2\kappa(O,O')$  (iii) ligands by (O4,5), (O18\*,19\*), O7 and O12, along with two water molecules (O10-Nd1-O11 68.70(2)). The Nd2 metal center coordinates to two oxygen atoms (O15,16) from a  $\kappa(O,O')$  carboxylate, six oxygens (O7#,8#), (O12,13), O5, and O18 from four  $\mu\text{-}1\kappa(O):2\kappa(O,O')$  carboxylate ligands, and two water oxygens (O21, O22; O21-Nd2-O22 69.97(2)).

The adjacent metal ions are linked by the bridging oxygens of  $Z_{L-1}$   $\mu$ -1 $\kappa$ (O):2 $\kappa$ (O,O') (iii) carboxylates forming a 1-D chain with angles of 115.294(17)° (Nd1-O5-Nd2), 116.726(17)° (Nd1-O12-Nd2), 115.098

(15)° (Nd1-O7-Nd2\*), and 115.319(16)° (Nd1-O18\*-Nd2\*). Along the chain, the angles about the metal ions are 169.893(3)° (Nd2-Nd1-Nd2\* and Nd1-Nd2-Nd1#), while the distances between the neighboring metal ions alternate between 4.3247(9) Å (Nd1-Nd2), and 4.3089(9) Å (Nd1-Nd2\* and Nd2-Nd1#). The mean Nd—O bond length with carboxylate ligands for both Nd1 and Nd2 is 2.542 Å and is higher than bond lengths with their coordinated  $\rm H_2O$  oxygens ( $\it cf.$  1).

Throughout the polymer chain, several hydrogen bond interactions can be observed as listed in Table S5. All lattice water molecules are involved in H-bonds in the crystal structure; O23 acts as a donor atom to hydroxyl O14; O24 and O25 are donors to hydroxyl O20 and coordinated O15 respectively, while also acting as acceptors to water O21 and O11 respectively; O26 acts as the donor atom to both O13 and O11#. Although both coordinated water molecules (O21, O22) of Nd2 make Hbonds, only one water molecule (O11) of Nd1 participates in hydrogen bonding. Unlike complexes 1, and 4-8 intra-ligand H-bonds are absent in this structure. In addition to those H-bonds formed by lattice waters within the same chain, these waters also form weak H bonding with adjacent chains, contributing to interchain interactions (Fig. S2). The crystallized waters of O26 and O24 form hydrogen bonds with OHgroup (O17 and O20 respectively) of neighboring chain ligands. Moreover, O23 lattice waters participate in hydrogen bonding with the other O23 lattice water molecules from other symmetries to link neibouring polymer chains through interactions with hydroxyl O14 of the ligands. (Note: symmetry codes have not been applied to atom labels for packing).

{  $[RE_2(2hpa)_6(H_2O)_2] \cdot 3H_2O$ }<sub>n</sub> (RE = Gd (4), Dy (5), Y (6), Er (7), Yb (8)): Complexes 4–8 are isomorphous and crystallize as one-dimensional polymers in the triclinic P-1 space group with a

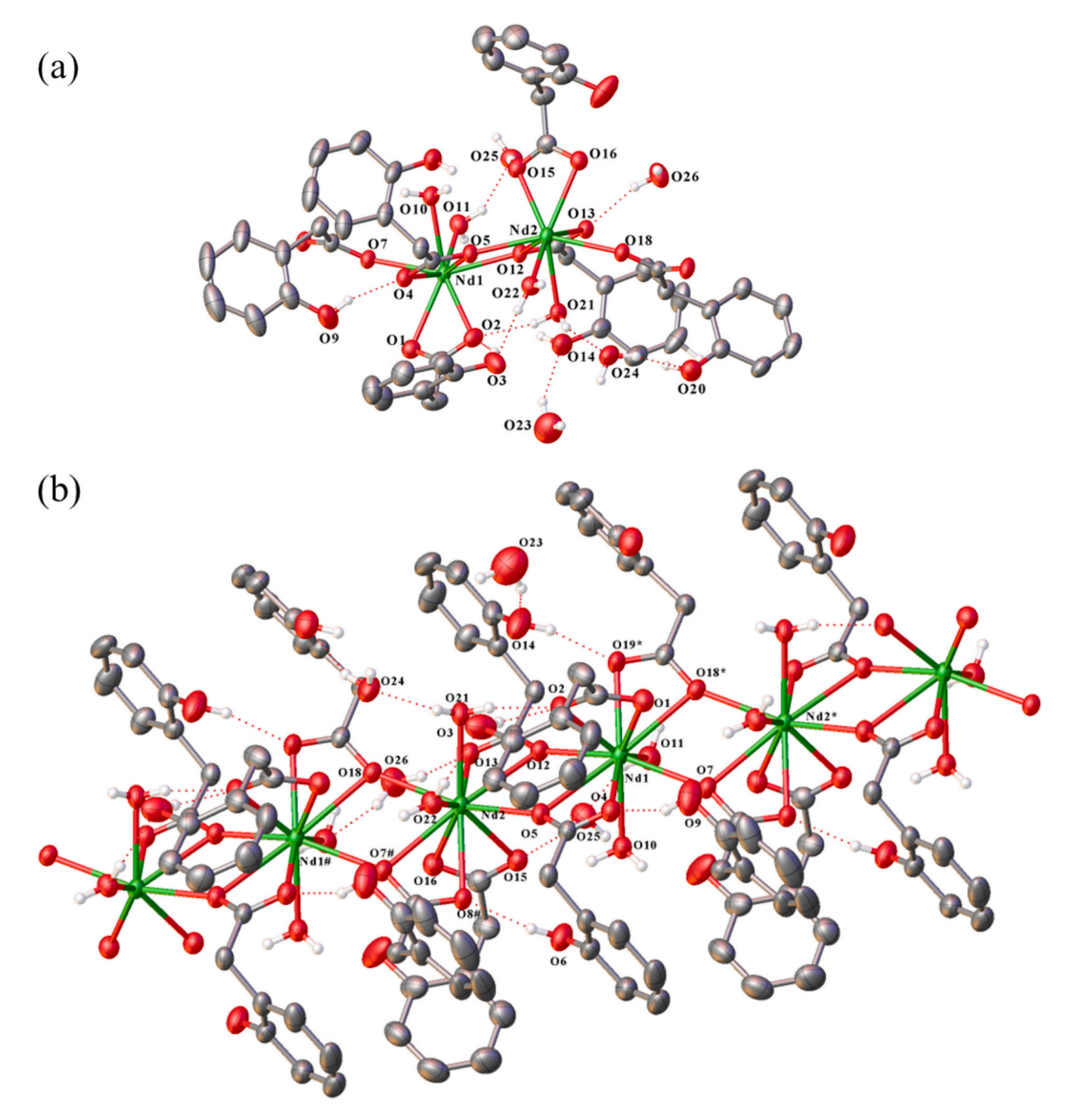


Fig. 4. (a) The asymmetric unit of  $\{[Nd_2(2hpa)_6(H_2O)_4]\cdot 3.5H_2O\}_n$  (3) (representative of complexes 2 and 3); (b) Part of the polymeric chain with 50 % thermal ellipsoids. Dotted lines indicate the intra-molecular hydrogen bonds. The hydrogen atoms, except those contributing to hydrogen bonds, and lattice water molecules are omitted for clarity. Selected bond lengths (Å) for 3: (Data for 2 in supplementary information): Nd1-O1 2.5686(7), Nd1-O2 2.5203(7), Nd1-O4 2.5141(7), Nd1-O5 2.6705(8), Nd1-O7 2.4490(7), Nd1-O10 2.5261(8), Nd1-O11 2.5108(8), Nd1-O12 2.4516(7), Nd1-O18\* 2.6473(8), Nd1-O19\* 2.5180(6), Nd2-O5 2.4469(7), Nd2-O12 2.6268(8), Nd2-O13 2.5170(7), Nd2-O15 2.5704(7), Nd2-O16 2.5508(7), Nd2-O18 2.4512(7), Nd2-O21 2.5017(8), Nd2-O22 2.5125(8), Nd2-O7# 2.6556(8), Nd2-O8# 2.5153(6). Symmetry codes: \*1 + X, +Y, +Z; #-1 + X, +Y, +Z.

bimetallic repeating unit. Fig. 5 depicts the asymmetric unit and a part of the polymeric chain of complex  $\{[Gd_2(2hpa)_6(H_2O)_2]\cdot 3H_2O\}_n$  (4) as representative. In the asymmetric unit, six 2-hydroxyphenylacetate ligands and two coordinated water molecules bind to two metal ions, and there are three waters (O21, O22, O23) of crystallization.

In the molecular structure, carboxylate ligands coordinate through only syn-syn-chelating bridging Z,Z- $\mu$ - $1\kappa(O)$ : $2\kappa(O,O')$  (iii) and syn-syn-bidentate bridging (i) modes. Both Gd1, and Gd2 metal centers are nine-coordinate in a tricapped trigonal prismatic geometry. The Gd1 metal ion builds its coordination environment with chelating oxygen atoms (O4,5) and (O16\*,17\*), as well as single oxygen atoms (O1 and O10)

from Z,Z- $\mu$ -1 $\kappa$ (O):2 $\kappa$ (O,O') (iii) ligands and (O7, and O1\*) from Z,Z- $\mu$ -1 $\kappa$ (O):2 $\kappa$ (O') (ii) carboxylates, along with one coordinated water molecule (O19). Four Z,Z- $\mu$ -1 $\kappa$ (O):2 $\kappa$ (O,O') (iii) carboxylates bind to Gd2 atom through (O10,11), (O1#,2#), O5, and O16, whilst there are two additional oxygen atoms (O8, and O13) from Z,Z- $\mu$ -1 $\kappa$ (O):2 $\kappa$ (O') carboxylate ligands. A single oxygen atom (O20) from a water molecule ligates Gd2 in the opposite direction to the water ligand of Gd1.

Neighboring metal centers are connected by two bridging oxygens (O5, O10 or O1, O16\*) of  $Z_iZ_{-\mu-1\kappa}(O):2\kappa(O,O')$  (iii) carboxylates and one  $Z_iZ_{-\mu-1\kappa}(O):2\kappa(O')$  (i) carboxylate through (O7, O8 or O13, O14). The distances between adjacent metal ions are 4.0688(3) Å, and 4.1051(3)

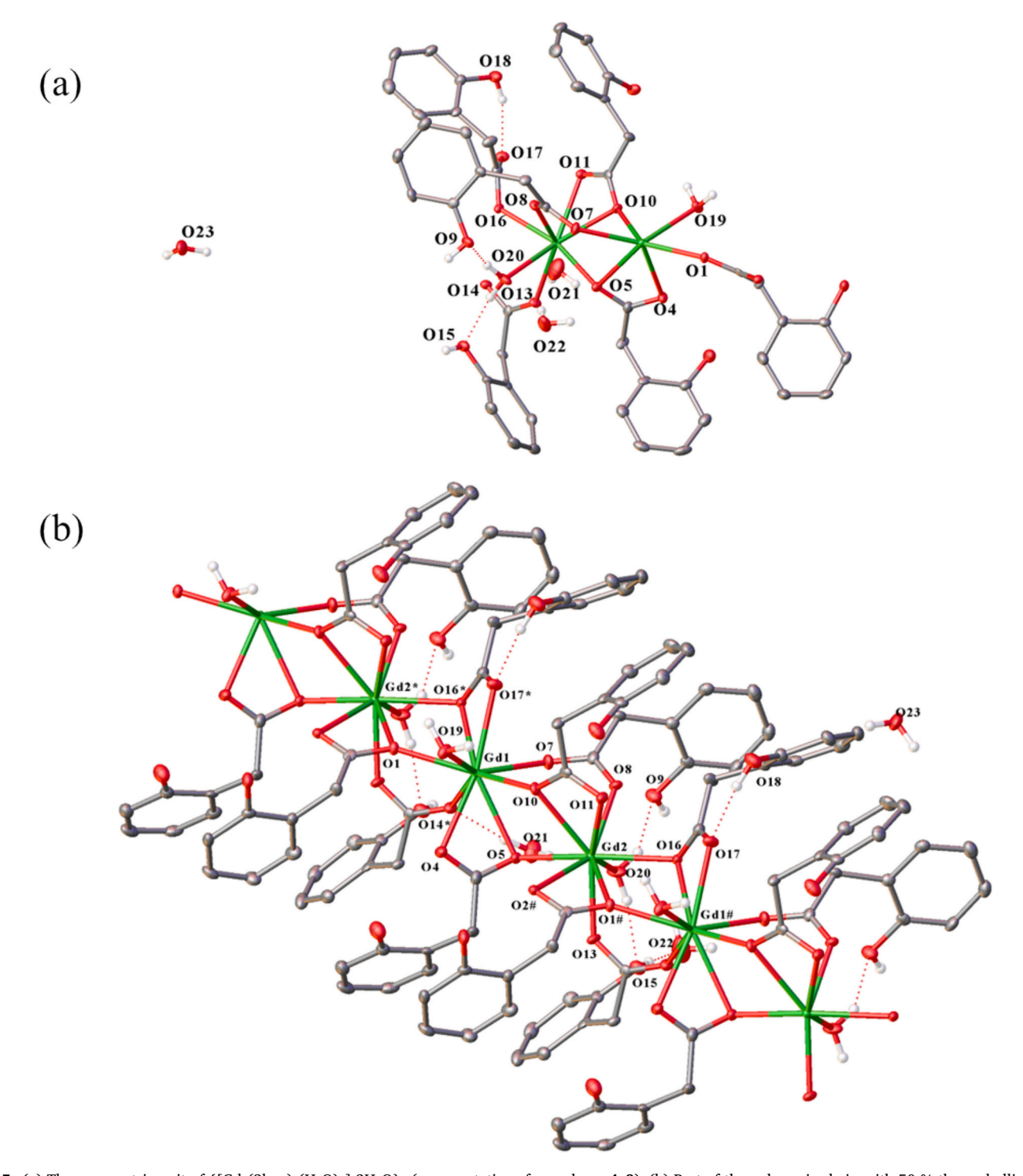


Fig. 5. (a) The asymmetric unit of  $\{[Gd_2(2hpa)_6(H_2O)_2]\cdot 3H_2O\}_n$  (representative of complexes 4–8); (b) Part of the polymeric chain with 50 % thermal ellipsoids. Dotted lines indicate the intra-molecular hydrogen bonds. The hydrogen atoms, except those contributing to hydrogen bonds, and lattice water molecules are omitted for clarity. Selected bond lengths (Å) for 4 (Data for 5–8 in supplementary information):  $Gd1-O1\ 2.37757(13)$ ,  $Gd1-O4\ 2.46107(14)$ ,  $Gd1-O5\ 2.60973(13)$ ,  $Gd1-O7\ 2.32601(11)$ ,  $Gd1-O1\ 2.37690(13)$ ,  $Gd2-O1\ 2.35548(11)$ ,  $Gd2-O1\ 2.51710(12)$ ,  $Gd2-O1\ 2.45406(13)$ ,  $Gd2-O1\ 3.34380(13)$ ,  $Gd2-O1\ 2.43092(13)$   $Gd2-O2\ 2.47734(16)$ ,  $Gd2-O1\ 2.52125(12)$ ,  $Gd2-O2\ 2.50023(13)$ . Symmetry codes: \*1 + X, +Y, +Z; #-1 + X, +Y, +Z.

Å, with a Gd2-Gd1-Gd2\* and Gd1-Gd2-Gd1# angle of 161.2872(16)° (Table S6). The average bond lengths of Gd1-O<sub>carboxylate</sub> and Gd2-O<sub>carboxylate</sub> are 2.458 Å and 2.439 Å respectively, with similar Gd-OH $_2$  bond lengths.

Two waters of crystallization form hydrogen bonds in the structure. O21 is a donor atom to the O14\* bridging oxygen, whereas O22 serves as

an acceptor to H from hydroxyl O15. The ligated water oxygen (O20) of the Gd2 metal center forms hydrogen bonds acting as a donor atom with two hydroxyl oxygens (O9 and O15). Moreover, one type of intramolecular H-bond interaction is formed between hydroxyl oxygen O18 and the chelating bridging carboxylate oxygen O17 (intra-ligand H-bonding). All intramolecular hydrogen bonds are illustrated in Fig. 5 and

their bond lengths and angles are listed in Table S7. In the packing of 1-D polymeric chains as presented in Fig. S3, O21 lattice waters connect adjacent chains by forming H-bonds with coordinated carboxylate O14 and hydroxyl O9 of two different chains. Similarly, O23 forms hydrogen bonds between coordinated water O19 and hydroxyl O6 of different neighboring chains. In addition, interligand hydrogen bonding between adjacent coordination polymers (between hydroxyl O12 and O18, and between hydroxyl O3 and coordinated carboxylate O2) further contribute to interchain interactions. (Note: symmetry codes have not been applied to atom labels for packing).

The metal ions with higher ionic radii (La, Ce, and Nd) acquire the coordination number of 10 along with the higher RE-O bond length, whereas metallic ions with smaller ionic radii (Gd, Dy, and Er) are 9-coordinate and have shorter bond lengths (Table 2). Across the series from La to Er, the average RE-O(carboxylate) bond lengths decrease, as shown in Table 2, consistent with the lanthanoid contraction [30].

#### 2.3. Corrosion inhibition evaluation

Weight Loss Measurements.

The calculated corrosion rates and the inhibition efficiencies of inhibitor compounds based on the immersion tests carried out in 0.01 M NaCl over 7 days are tabulated in Table 3. At the end of the period, all inhibitor-treated coupons exhibited comparatively less corrosion than the control. They all exhibited a brownish yellow colour all over the metal coupons, unlike the control specimens (Fig. S8), and that is explicable by the attachment of the complexes to the oxidized metal surface. This may occur through Fe-OH condensing with the 2-hydroxy group of the ligand, bridging of the carboxylate between the rare earth and iron, and ligation of the surface OH groups to the rare earth, thereby forming a surface protective film which consists of a mixture of ligands, RE and Fe oxides/hydroxides [11,25]. The corrosion inhibition properties of these compounds were compared with [Ce(salH)<sub>3</sub>(H<sub>2</sub>O)]<sub>n</sub>, one of the earliest RE carboxylate inhibitors reported [15] under similar conditions. It is well established that lanthanoid salts and sodium carboxylate perform less well than lanthanoid carboxylates [10,15,18,24,31]. Furthermore, a mixture of rare earth salt and sodium 2-hydroxyphenylacetate can lead to a precipitation and in any case such mixtures have been evaluated for other analogous systems and do not outperform preformed complexes. They complicate the results due to the presence of a sodium salt as a biproduct.

According to the weight loss experimental results (Table 3), the La (1), Nd (3), and Yb (8) complexes perform as well as  $[Ce(salH)_3(H_2O)]_n$  with the highest inhibition efficiency at 57 % shown by 4, and the

Table 2 Coordination numbers, carboxylate ligation and average RE-O $_{carboxylate}$  bond lengths for compounds 1–7.

Complex	RE atom	CN	Ligation	Avg. bond length RE-O <sub>carboxylate</sub> (Å)
$[La(2hpa)_3(H_2O)_2]_n$ (1)	La1	10	$[1 \times (ii)], [2 \times (iii)^{1}], [2 \times (iii)^{2}], [2 \times H_{2}O]$	2.594
$\{[RE_2(2hpa)_6(H_2O)_4]\cdot$	RE1	10	$[1 \times (ii)], [2 \times$	Ce1-2.571
$3.5H_{2}O_{n}$			(iii) <sup>1</sup> ], [2 $\times$	Nd1-2.542
(RE = Ce (2), Nd (3))			(iii) <sup>2</sup> ], [2 × $H_2O$ ]	
	RE2	10	[2 $\times$ (ii)], [2 $\times$	Ce2-2.570
			$(iii)^1$ ], $[2 \times$	Nd2-2.542
			$(iii)^2$ ], $[2 \times H_2O]$	
$\{[RE_2(2hpa)_6(H_2O)_2]\cdot$	RE1	9	$[2 \times (i)], [2 \times$	Gd1-2.458
$3H_2O$ <sub>n</sub>			$(iii)^1$ ], [2 ×	Dy1-2.437
(RE = Gd (4), Dy (5),			$(iii)^2$ ], $[1 \times H_2O]$	Er1-2.419
Er (7))				
	RE2	9	$[2 \times (i)], [2 \times$	Gd2-2.439
			$(iii)^1$ ], $[2 \times$	Dy2-2.417
			$(iii)^2$ ], $[1 \times H_2O]$	Er2-2.397

Note: (iii)1 – unidentate (iii)2 – chelating.

**Table 3**Corrosion rates (mm/year) and percentage inhibition efficiency (IE%) of compounds **1–8** for mild in 0.01 M NaCl.

Solution	Conce	ntration	Average weight loss percentage (%)	Corrosion Rate (mm/ year)	IE %
	ppm	mM	· <u> </u>		_
Control	580	10	0.18	0.098	-
$[La(2hpa)_3(H_2O)_2]_n$ 1	500	0.796	0.09	0.050	50
{[Ce(2hpa) <sub>6</sub> (H <sub>2</sub> O) <sub>4</sub> ]· 3.5H <sub>2</sub> O} <sub>n</sub> <b>2</b>	500	0.380	0.13	0.074	24
$\{[Nd_2(2hpa)_6(H_2O)_4]\cdot 3.5H_2O\}_n$ 3	500	0.378	0.09	0.051	48
$\{[Gd_2(2hpa)_6(H_2O)_2]\cdot 3H_2O\}_n$ 4	500	0.381	0.08	0.043	57
$\{[Dy_2(2hpa)_6(H_2O)_2]\cdot 3H_2O\}_n$ 5	500	0.378	0.11	0.059	40
$\{[Y_2(2hpa)_6(H_2O)_2]\cdot 3H_2O\}_n$ <b>6</b>	500	0.426	0.13	0.073	26
$\{[Er_2(2hpa)_6(H_2O)_2]\cdot 3H_2O\}_n$ 7	500	0.376	0.11	0.062	37
$\{[Yb_2(2hpa)_6(H_2O)_2]\cdot 3H_2O\}_n$ 8	500	0.372	0.09	0.049	50
[Ce(salH) <sub>3</sub> (H <sub>2</sub> O)] <sub>n</sub>	500	0.878	0.09	0.052	48

minimum inhibition (24 %) by the Ce complex (2). In the cases of La, Gd and Dy complexes, the inhibition was better than those of the corresponding unsubstituted phenylacetate analogues [13], but no enhancement was observed for Nd. Thus, introduction of the 2-hydroxy substituent was mainly advantageous. However, the inhibition properties of the RE 2- hydroxyphenylacetate complexes are inferior compared to the RE complexes of 4- hydroxyphenylacetate [25] where the introduction of the 4-hydroxy substituent into phenylacetate had a major effect. Moreover, cerium salicylate is no longer the benchmark for optimum corrosion inhibition performance by rare earth carboxylates, having been superseded by lanthanum 4-hydroxycinnamate [10], vttrium 3-(4'-methylbenzoyl)propanoate [19,20], and vttrium 4-hydroxybenzoate [22]. Owing to the indifferent corrosion inhibition performance of RE 2- hydroxyphenylacetate compounds, potentiodynamic polarization (PP) testing for electrochemical evaluation was not conducted. Nevertheless, these results highlight the impact of the position of the hydroxyl group in hydroxyphenylacetate complexes on their corrosion inhibition performances. Together with earlier studies of the 4hydroxyphenylacetates, these results indicate the positive effect of adding a hydroxyl group to phenylacetate on inhibitor performance and the importance of its location. Whereas the insertion of a methylene linker reduced inhibitor performance from that of 4-hydroxybenzoate [25], its impact on salicylate appears to be minimal except for Ce.

## 3. Conclusions

Three different 1-D coordination polymeric structures were obtained by the synthesis of a series of rare earth agua 2-hydroxyphenylacetate complexes by the salt metathesis reaction. Except for the La complex, the others 2-8 are based on binuclear repeating units and the crystal structures have waters of crystallization. For all three structural types, the chelating bridging carboxylate coordination mode is dominant and La, Ce, Nd complexes also exhibit chelating bidentate binding while 4-8 also have the syn-syn-bridging bidentate mode. As a result of the lanthanoid contraction within the series, the complexes of higher ionic radii metals are 10 coordinate and of lower ionic radii metals have 9 coordination. The average RE-O(carboxylate) bond lengths decrease within the series 1–8. The introduction of a 2-hydroxy group into phenylacetate increases the structural classes from two to three, but not owing to HO-RE coordination. However, the 2-OH group is involved in extensive Hbonding. Neither these compounds nor [Ce(salH)<sub>3</sub>(H<sub>2</sub>O)] outperformed the anti-corrosion properties of rare earth 4-hydroxyphenylacetates for mild steel in a mild corrosive environment. Their corrosion inhibition

efficiencies were less than that of the lowest value for RE 4-hydroxyphenylacetates [25]. In the present case, the  $-CH_2$ -linker has little impact on corrosion inhibition properties, except the adverse effect with Ce.

## 4. Experimental

#### 4.1. General considerations

Standard commercially available reagents and solvents were used for the syntheses without further purification. 2-hydroxyphenylacetic acid purchased from Fluorochem or Sigma-Aldich and rare earth metal salts were from Sigma-Aldrich. Powder X-ray diffraction patterns were obtained at room temperature with a Bruker D2 PHASER diffractometer in the range of 3–50° of 20 with a 0.2° or 0.1° divergence slit and at 0.02° increments. The Mercury program provided by the Cambridge Crystallographic Data Centre was used to generate the simulated powder patterns of the complexes based on their single-crystal XRD data. IR spectra were obtained within the region 4000–500 cm<sup>-1</sup> by a Nicolet<sup>TM</sup> iS<sup>TM</sup> 5 FTIR Spectrometer. Samples were sent to the Microanalytical Laboratory at the Science Centre, London Metropolitan University, England to carry out the elemental analyses (C, H). Metal analyses were done through complexometric titration between 0.0100 M EDTA and an aqueous metal ion solution in the presence of Xylenol Orange indicator and hexamethylenetetramine buffer. The aqueous metal ion solution was prepared by dissolving the compound in distilled water and the addition of few milliliters of dilute HCl. Thermal stability of the compounds was determined by Thermogravimetric analysis (TGA), with a TA instrument SDT 650 in the temperature range from room temperature to 750 °C with a ramp of 10 °C min<sup>-1</sup>. The tests were conducted under a N<sub>2</sub> atmosphere at a flow rate of 50 mLmin<sup>-1</sup> and using standard 90 μL alumina sample pans. Melting points were determined in a glass capillary tube and are reported without calibration. Crystal data and refinement details are given in Table S1. CCDC 2444923-2444926 for compounds 1-4, 2444927 for compound 5, and 2444928 for compound 7, contain the supplementary crystallographic data for this paper. These data can be obtained free of charge from The Cambridge Crystallographic Data Centre via www.ccdc.cam.ac.uk/data request/cif.

## 4.2. Synthesis of RE 2-hydroxyphenylacetate (RE-2hpa) complexes

A few drops of 95 % ethanol and about 3 mL of distilled water were added to 2-hydroxyphenyl acetic acid (1.5 mmol) powder. An equimolar amount of sodium hydroxide (1.5 mmol) in 6 mL of distilled water was added to the partially dissolved ligand and the reaction mixture was shaken until the ligand dissolved completely whilst maintaining the pH within 7–8. Then the stoichiometric amount of rare earth metal chloride or nitrate salt in water was slowly treated with the sodium 2-hydroxyphenyl acetate solution and stirred for 1 h at pH 5–6. The resultant powder or slightly cloudy solution was gravity filtered and the mother liquor grew crystals by slow evaporation. The precipitate and crystals were washed with mixture of ethanol and distilled water before air drying. The yield was calculated on the basis of the number of moles of rare earth salt used, for the mixture of crystals and powder where both were isolated or just crystals in other cases.

1:[La(2hpa) $_3$ (H $_2$ O) $_2$ ] $_n$  White crystals and white powder; Yield: 0.256 g, 86 %. Analyses were carried out for mixture of crystals and powder. m.p. 206 °C (dec). Elemental analysis for C $_2$ 4H $_2$ 5LaO $_1$ 1 (MW: 628.35 gmol $^{-1}$ ): Calculated (%) C 45.88, H 4.01, La 22.11; Found (%) C 45.64, H 3.67, La 22.26. IR (cm $^{-1}$ ): 3226 br w, 1584 w, 1546 m, 1517 s, 1489 m, 1459 w, 1430 s, 1406 m, 1341 w, 1254 w, 1239 w, 1218 m, 1163 m, 1098 w, 1038 w, 958 w, 941 w, 878 w, 792 w, 745 s, 712 m, 647 m, 573 m, 544 m, 511 m. TGA weight loss (25–125 °C); 6.0 % (Calc. for loss of 2 × H $_2$ O = 5.7 %).

2:{ $[Ce_2(2hpa)_6(H_2O)_4]\cdot 3.5H_2O\}_n$  White crystals and salmon pink powder; Yield: 0.329 g, 100 %. Analyses were carried out only for crystals. m.p. 196–198 °C (dec). Elemental analysis for  $C_{48}H_{57}Ce_2O_{25.5}$ 

(MW:  $1322.17 \text{ gmol}^{-1}$ ): Calculated (%) C 43.60, H 4.35, Ce 21.19; Found (%) C 43.42, H 3.81, Ce 21.44. IR (cm<sup>-1</sup>): 3277 br w, 1586 m, 1551 m, 1519 s, 1488 m, 1458 m, 1417 s, 1328 m, 1284 w, 1246 m, 1209 m, 1155 m, 1096 m, 1038 w, 957 w, 942 w, 875 w, 848 w, 798 w, 744 s, 710 s, 695 m, 651 s, 619 m, 573 s, 548 s. TGA weight loss  $(25-105\,^{\circ}\text{C})$ ; 9.8 % (Calc. for loss of  $7.5 \times \text{H}_2\text{O} = 10.3 \text{ %}$ ).

3:{[Nd<sub>2</sub>(2hpa)<sub>6</sub>(H<sub>2</sub>O)<sub>4</sub>]·3.5H<sub>2</sub>O}<sub>n</sub> Puple crystals; Yield: 0.321 g, 97 %. m.p. 210–212 °C (dec). Elemental analysis for  $C_{48}H_{57}Nd_2O_{25.5}$  (MW: 1330.41 gmol<sup>-1</sup>): Calculated (%) C 43.33, H 4.32, Nd 21.68; Found (%) C 43.53, H 3.84, Nd 21.66. IR (cm<sup>-1</sup>): 3269 br w, 1586 w, 1551 m, 1519 m, 1488 m, 1425 s, 1329 w, 1284 w, 1256 m, 1210 m, 1156 m, 1096 w, 1038 w, 958 w, 942 w, 875 w, 848 w, 800 w, 744 s, 711 m, 695 m, 659 m, 619 m, 574 m, 549 m. TGA weight loss (25–110 °C); 10.1 % (Calc. for loss of 7.5  $\times$  H<sub>2</sub>O = 10.2 %).

4: {[Gd<sub>2</sub>(2hpa)<sub>6</sub>(H<sub>2</sub>O)<sub>2</sub>]·3H<sub>2</sub>O}<sub>n</sub> Brownish-white crystals; Yield: 0.271 g, 83 %. m.p. 215 °C (dec). Elemental analysis for  $C_{48}H_{52}Gd_2O_{23}$  (MW: 1311.39 gmol<sup>-1</sup>): Calculated (%) C 43.96, H 4.00, Gd 23.98; Found (%) C 43.69, H 3.36, Gd 24.31. IR (cm<sup>-1</sup>): 3589 w, 3153 br w, 1589 w, 1561 m, 1527 s, 1491 m, 1458 m, 1419 s, 1314 m, 1292 m, 1272 w, 1240 m, 1168 m, 1099 m, 1040 w, 955 w, 932 w, 876 w, 850 w, 798 m, 745 s, 709 m, 698 m, 626 m, 580 m, 545 m, 535 m. TGA weight loss (25–150 °C): 7.4 % (Calc. for loss of 5 ×  $H_2O$  = 6.9 %).

5:{[Dy<sub>2</sub>(2hpa)<sub>6</sub>(H<sub>2</sub>O)<sub>2</sub>]·3H<sub>2</sub>O}<sub>n</sub> White crystals; Yield: 0.257 g, 78 %. m.p. 191–192 °C (dec). Elemental analysis for  $C_{48}H_{52}Dy_2O_{23}$  (MW: 1321.89 gmol  $^{-1}$ ): Calculated (%) C 43.61, H 3.96, Dy 24.59; Found (%) C 43.17, H 3.36, Dy 24.46. IR (cm  $^{-1}$ ): 3589 w, 3159 br w, 1589 w, 1566 m, 1527 s, 1491 m, 1458 m, 1421 s, 1315 m, 1292 m, 1272 w, 1241 m, 1215 m,1168 m, 1100 m, 1040 w, 955 w, 933 w, 876 w, 850 w, 799 w, 746 s, 710 m, 699 m, 626 m, 581 m, 544 m, 535 m. TGA weight loss (25–110 °C); 6.0 % (Calc. for loss of 5 ×  $H_2O$  = 6.8 %).

6:{[Y<sub>2</sub>(2hpa)<sub>6</sub>(H<sub>2</sub>O)<sub>2</sub>]·3H<sub>2</sub>O}<sub>n</sub> Brownish-white crystals; Yield: 0.209, 71 % m.p. 112–114 °C (dec). Elemental analysis for  $C_{48}H_{52}O_{23}Y_2$  (MW: 1174.72 gmol<sup>-1</sup>): Calculated (%) C 49.08, H 4.46, Y 15.14; Found (%) C 48.97, H 3.99, Y 14.72. IR (cm<sup>-1</sup>): 3599 w, 3171 br w, 1589 w, 1570 m, 1528 m, 1489 m, 1458 m, 1425 m, 1315 w, 1292 w, 1271 w, 1241 m, 1215 m, 1169 w, 1100 w, 1072 w, 1040 w, 956 w, 932 w, 877 w, 850 w, 799 w, 747 s, 699 m, 626 m, 582 m, 545 m, 528 m. TGA weight loss (25–110 °C); 8.0 % (Calc. for loss of 5 × H<sub>2</sub>O = 7.7 %). 6 crystallized in the triclinic space group *P*-1, a = 8.0100(5), b = 15.830 (1), c = 20.0400(13), a = 70.478(2)°,  $\beta$  = 82.121(2)°,  $\gamma$  = 80.325(3)°, similar to 4, 5 and 7.

7:{[Er<sub>2</sub>(2hpa)<sub>6</sub>(H<sub>2</sub>O)<sub>2</sub>]·3H<sub>2</sub>O}<sub>n</sub> Pink crystals; Yield: 0.218 g, 66 %. m.p. 243–245 °C (dec). Elemental analysis for  $C_{48}H_{52}Er_2O_{23}$  (MW: 1331.41 gmol<sup>-1</sup>): Calculated (%) C 43.30, H 3.94, Er 25.12; Found (%) C 43.24, H 3.63, Er 25.02. IR (cm<sup>-1</sup>): 3595 w, 3157 br w, 1589 w, 1567 m, 1527 m, 1492 m, 1458 m, 1421 s, 1315 m, 1292 m, 1271 w, 1241 m, 1215 m, 1168 m, 1100 m, 1040 w, 957 w, 933 w, 876 w, 850 w, 799 w, 746 s, 710 m, 699 m, 626 m, 582 m, 544 m, 535 m. TGA weight loss (25–115 °C); 7.5 % (Calc. for loss of 5 ×  $H_2O = 6.8$  %).

**8**:{[Yb<sub>2</sub>(2hpa)<sub>6</sub>(H<sub>2</sub>O)<sub>2</sub>]·3H<sub>2</sub>O}<sub>n</sub> White microcrystalline solid; Yield: 0.182 g, 54 %. m.p.  $100\,^{\circ}\text{C}$  (dec). Elemental analysis for  $\text{C}_{48}\text{H}_{52}\text{O}_{23}\text{Yb}_2$  (MW:  $1342.99~\text{gmol}^{-1}$ ): Calculated (%) C 42.93, H 3.90, Yb 25.77; Found (%) C 42.59, H 3.61, Yb 25.45. IR (cm<sup>-1</sup>): 3601 w, 3153 br w, 1570 m, 1528 s, 1492 m, 1458 m, 1425 s, 1316 m, 1293 m, 1271 w, 1241 m, 1215 m, 1169 m, 1100 m, 1040 w, 957 w, 934 w, 876 w, 850 w, 800 m, 746 s, 711 m, 700 m, 626 m, 583 m, 544 m, 535 m. TGA weight loss (25–100 °C); 6.6 % (Calc. for loss of  $5\times\text{H}_2\text{O}=6.7$  %). **8** crystallized in the triclinic space group *P*-1, a=7.9900(16), b=15.830(3), c=20.050(4),  $a=70.46(3)^{\circ}$ ,  $\beta=82.03(3)^{\circ}$ ,  $\gamma=80.26(3)^{\circ}$ , similar to **4**, 5 and **7**.

## 4.3. Weight loss testing

The weight loss method was carried out to estimate the corrosion inhibition properties of the synthesized compounds following the standard method ASTM G1-03 [32] and G31-72 [33]. Mild-steel alloy AS

1020 coupons with dimensions of approximately  $20\times20\times3$  mm were used as test specimens. The test was duplicated for each inhibition compound and the control. The corrosion rates (R) of the inhibitor solutions and the control were calculated using the Eq. 2 and the average of measurements is reported.

Corrosion Rate (R) = 
$$(K \times W)/A \times T \times D$$
 (2)

where K is a constant ( $K = 8.76 \times 10^4$ ); W is the weight loss (g); A is the coupon area (cm<sup>2</sup>); T is the time of exposure (168 h); D is the density of the coupon material (7.87 g/cm<sup>3</sup>).

Then the percentage corrosion inhibition efficiency (IE%) of each compound solution at a given concentration, was determined relative to the control test using Eq. 3.

## CRediT authorship contribution statement

Naveena Y. Salpadoru Thuppahige: Writing – original draft, Validation, Investigation, Formal analysis, Data curation. Zhifang Guo: Writing – review & editing, Writing – original draft, Validation, Investigation, Formal analysis, Data curation. Glen B. Deacon: Writing – review & editing, Writing – original draft, Supervision, Project administration, Methodology, Funding acquisition, Formal analysis, Conceptualization. Peter C. Junk: Writing – review & editing, Supervision, Resources, Project administration, Methodology, Funding acquisition, Conceptualization.

## **Author statement**

**Naveena Y. Salpadoru Thuppahige** performed most of the synthetic and characterization work in this paper, wrote the initial draft of the paper and was involved in subsequent drafts for completion of the paper.

**Zhifang Guo** was primarily involved with all the Xray work in the paper, but also helped with the initial draft and subsequent drafts of the paper

**Glen B. Deacon** was involved with the ideas and acquisition of funding for the paper and also heavily involved in final drafts of the paper.

**Peter C. Junk** was involved with the ideas and acquisition of funding for the paper and also involved in final drafts of the paper, along with supervision for the project.

## Declaration of competing interest

The authors declare that they have no known competing financial interests or personal relationships that could have appeared to influence the work reported in this paper.

## Acknowledgements

PCJ and GBD gratefully acknowledge the ARC for funding (DP200100568). PCJ and ZG acknowledge James Cook University for internal funding. Parts of this research were undertaken on the MX1 beamline at the Australian Synchrotron, part of ANSTO [34].

## Appendix A. Supplementary data

Supplementary data to this article can be found online at https://doi.org/10.1016/j.ica.2025.122796.

## Data availability

The data that support the findings of this study are available in the

supplementary material of this article.

#### References

- [1] T. Behrsing, G.B. Deacon, P.C. Junk, The chemistry of rare-earth metals, in: The Lanthanides and Actinides: Synthesis, Reactivity, Properties and Applications, World Scientific Publishing Europe Ltd, London, 2022, pp. 1–36, https://doi.org. 10.1142/9781800610163 0001.
- [2] A. Cârâc, Biological and biomedical applications of the lanthanides compounds: a Mini review, Proc. Rom. Acad., Ser. B:Chem., Life Sci. Geosci. 19 (2017) 69–74, in: http://www.acad.ro/sectii2002/proceedingsChemistry/doc2017-2/art01.pdf.
- [3] R. Wang, Z. Zheng, Rare earth complexes with carboxylic acids, Polyaminopolycarboxylic acids, and amino acids, in: Rare Earth Coordination Chemistry: Fundamentals and Applications, John Wiley & Sons (Asia) Pte Ltd., Singapore, 2010, pp. 91–136, https://doi.org/10.1002/9780470824870.ch3.
- [4] R. Janicki, A. Mondry, P. Starynowicz, Carboxylates of rare earth elements, Coord. Chem. Rev. 340 (2017) 98–133, https://doi.org/10.1016/j.ccr.2016.12.001.
- [5] A. Fischbach, F. Perdih, E. Herdtweck, R. Anwander, Structure reactivity relationships in rare-earth metal carboxylate-based binary Ziegler-type catalysts, Organometallics 25 (2006) 1626–1642, https://doi.org/10.1021/om060052i.
- [6] P. Mahata, K.V. Ramya, S. Natarajan, Synthesis, structure and optical properties of rare-earth benzene carboxylates, Dalton Trans. 36 (2007) 4017–4026, https://doi. org/10.1039/b706363f.
- [7] A.J. Amoroso, S.J.A. Pope, Using lanthanide ions in molecular bioimaging, Chem. Soc. Rev. 44 (2015) 4723–4742, https://doi.org/10.1039/c4cs00293h.
- [8] J.A. Peters, J. Huskens, D.J. Raber, Lanthanide induced shifts and relaxation rate enhancements, Prog. Nucl. Magn. Reason. Spectrosc. 28 (1996) 283–350, https:// doi.org/10.1016/0079-6565(95)01026-2.
- [9] H.M. Ren, H.W. Wang, Y.F. Jiang, Z.X. Tao, C.Y. Mu, G. Li, Proton Conductive Lanthanide-Based Metal-Organic Frameworks: Synthesis Strategies, Structural Features, and Recent Progress, Top. Curr. Chem. 380 (2022) 9, https://doi.org/ 10.1007/s41061-022-00367-9.
- [10] M. Forsyth, M. Seter, B. Hinton, G. Deacon, P. Junk, New 'green' corrosion inhibitors based on rare earth compounds, Aust. J. Chem. 64 (2011) 812–819, https://doi.org/10.1071/CH11092.
- [11] Y. Peng, A.E. Hughes, J.I. Mardel, G.B. Deacon, P.C. Junk, R.A. Catubig, M. Forsyth, B.R.W. Hinton, A.E. Somers, Dual function of rare earth carboxylate compounds on the barrier properties and active corrosion inhibition of epoxy coatings on mild steel, Prog. Org. Coat. 185 (2023) 107870, https://doi.org/ 10.1016/j.porgcoat.2023.107870.
- [12] T. Behrsing, G.B. Deacon, J. Luu, P.C. Junk, B.W. Skelton, A.H. White, Structural diversity of lanthanoid salicylate hydrates, Polyhedron 120 (2016) 69–81, https:// doi.org/10.1016/j.poly.2016.05.047.
- [13] E. Mottram, S. Hamilton, J.S. Moon, J. Wang, G. Bousrez, A.E. Somers, G. B. Deacon, P.C. Junk, Synthesis, structure, and corrosion inhibiting properties of phenylacetato-rare earth(III) complexes, J. Coord. Chem. 73 (2020) 2677–2697, https://doi.org/10.1080/00958972.2020.1839894.
- [14] M. Forsyth, C.M. Forsyth, K. Wilson, T. Behrsing, G.B. Deacon, ATR characterisation of synergistic corrosion inhibition of mild steel surfaces by cerium salicylate, Corros. Sci. 44 (2002) 2651–2656, https://doi.org/10.1016/S0010-938X(02)00024-0.
- [15] M. Forsyth, K. Wilson, T. Behrsing, C. Forsyth, G.B. Deacon, A. Phanasgoankar, Effectiveness of rare-earth metal compounds as corrosion inhibitors for steel, Corrosion 58 (2002) 953–960, https://doi.org/10.5006/1.3280785.
- [16] M. Forsyth, M. Seter, M.Y. Tan, B. Hinton, Recent developments in corrosion inhibitors based on rare earth metal compounds, Corros, Eng., Sci. Technol. 49 (2014) 130–135, https://doi.org/10.1179/1743278214Y.0000000148.
- [17] V.P. Vithana, Z. Guo, G.B. Deacon, P.C. Junk, Rare earth 2-Methyl-3-furoate complexes: effect of steric hindrance on corrosion inhibitor properties, Eur. J. Inorg. Chem. 27 (2024) e202300722, https://doi.org/10.1002/ejic.202300722.
- [18] F. Blin, S.G. Leary, K. Wilson, G.B. Deacon, P.C. Junk, M. Forsyth, Corrosion mitigation of mild steel by new rare earth cinnamate compounds, J. Appl. Electrochem. 34 (2004) 591–599, https://doi.org/10.1023/B: JACH.0000021932.87043.7b.
- [19] Y. Peng, A.E. Hughes, G.B. Deacon, P.C. Junk, B.R.W. Hinton, M. Forsyth, J. I. Mardel, A.E. Somers, A study of rare-earth 3-(4-methylbenzoyl)-propanoate compounds as corrosion inhibitors for AS1020 mild steel in NaCl solutions, Corros. Sci. 145 (2018) 199–211, https://doi.org/10.1016/j.corsci.2018.09.022.
- [20] A.E. Somers, B.R.W. Hinton, C. de Bruin-Dickason, G.B. Deacon, P.C. Junk, M. Forsyth, New, environmentally friendly, rare earth carboxylate corrosion inhibitors for mild steel, Corros. Sci. 139 (2018) 430–437, https://doi.org/ 10.1016/j.corsci.2018.05.017.
- [21] V.P. Vithana, Z. Guo, G.B. Deacon, A.E. Somers, P.C. Junk, RE(III) 3-Furoate complexes: synthesis, structure, and corrosion inhibiting properties, Molecules 27 (2022) 8836, https://doi.org/10.3390/molecules27248836.
- [22] J. Moon, Z. Guo, O.A. Beaumont, S. Hamilton, G. Bousrez, E. Mottram, J. Wang, A. E. Somers, G.B. Deacon, P.C. Junk, 4-Hydroxybenzoato-rare earth(iii) complexes-syntheses, a structural goldmine from coordination diversity and improved corrosion inhibition behaviour, New J. Chem. 47 (2023) 16843–16854, https://doi.org/10.1039/d3nj02735j.
- [23] V.P. Vithana, Z. Guo, G.B. Deacon, A.E. Somers, P.C. Junk, Synthesis, structure, and corrosion inhibiting properties of REIII 3-thiophenecarboxylate complexes, New J. Chem. 46 (2022) 19104–19111, https://doi.org/10.1039/d2nj03556a.

- [24] G.B. Deacon, P.C. Junk, W.W. Lee, M. Forsyth, J. Wang, Rare earth 3-(4'-hydroxyphenyl)propionate complexes, New J. Chem. 39 (2015) 7688–7695, https://doi.org/10.1039/c5nj00787a.
- [25] N.Y. Salpadoru Thuppahige, Z. Guo, G.B. Deacon, A.E. Somers, P.C. Junk, Rare-earth 4-Hydroxyphenylacetate complexes: synthesis, structural characterization, and corrosion inhibition properties, Z, Z. Anorg. Allg. Chem. 651 (2025) e202400180, https://doi.org/10.1002/zaac.202400180.
- [26] A. Aragón-Muriel, M. Camprubí-Robles, E. González-Rey, A. Salinas-Castillo, A. Rodríguez-Diéguez, S. Gómez-Ruiz, D. Polo-Cerón, Dual investigation of lanthanide complexes with cinnamate and phenylacetate ligands: study of the cytotoxic properties and the catalytic oxidation of styrene, Polyhedron 80 (2014) 117–128, https://doi.org/10.1016/j.poly.2014.02.040.
- [27] H. Zhang, G.Y. Liu, X.H. Diao, Y. Muhammad, C. Chen, Y.Y. Gao, H. Wang, C.S. Qi, W. Li, A series of isostructural In-based coordination polymers: crystal structure, luminescence sensing and color tuning, J. Solid State Chem. 324 (2023) 124114, https://doi.org/10.1016/j.jssc.2023.124114.
- [28] G.B. Deacon, R.J. Phillips, Relationships between the carbon-oxygen stretching frequencies of carboxylato complexes and the type of carboxylate coordination, Coord. Chem. Rev. 33 (1980) 227–250, https://doi.org/10.1016/S0010-8545(00) 80455-5

- [29] K. Nakamoto, Applications in Coordination Chemistry, in: Infrared and Raman Spectra of Inorganic and Coordination Compounds: Part B: Applications in Coordination, Organometallic, and Bioinorganic Chemistry, John Wiley & Sons, Inc. New Jersey, 2009, pp. 1–273, https://doi.org/10.1002/9780470405888.ch1.
- [30] R.D. Shannon, Revised effective ionic radii and systematic studies of interatomic distances in halides and chalcogenides, Acta Crystallogr. A32 (1976) 751–767, https://doi.org/10.1107/80567739476001551.
- [31] V.P. Vithana, Z. Guo, G.B. Deacon, P.C. Junk, Syntheses, structures, and corrosion inhibition of various alkali metal carboxylate complexes, Molecules 28 (2023) 5515, https://doi.org/10.3390/molecules28145515.
- [32] ASTM GI-03, Standard practice for preparing, cleaning, and evaluating corrosion test specimens, ASTM, International (2017), https://doi.org/10.1520/G0001-03R17F01
- [33] ASTM G31-72, Standard practice for laboratory immersion corrosion testing of metals, ASTM, International (2004), https://doi.org/10.1520/G0031-72R04.
- [34] N.P. Cowieson, D. Aragao, M. Clift, D.J. Ericsson, C. Gee, S.J. Harrop, N. Mudie, S. Panjikar, J.R. Price, A. Riboldi-Tunnicliffe, R. Williamson, T. Caradoc-Davies, MX1: a bending-magnet crystallography beamline serving both chemical and macromolecular crystallography communities at the Australian Synchrotron, Synchrotron Radiation 22 (2015) 187–190, https://doi.org/10.1107/S1600577514021717.